5
Organic Nanophotonics: Controllable Assembly of Optofunctional Molecules toward Low-Dimensional Materials with Desired Photonic Properties

Yongli Yan and Yong Sheng Zhao

5.1
Introduction

Nanophotonics, which deals with the generation, transfer, modulation, and detection of photons in a confined system, was first introduced in the near-field optics/spectroscopy, and subsequently generalized in other fields such as photonic crystals and surface plasmon optics and materials [1]. In comparison with electrons, photons exhibit great superiority as information carriers, including speed, bandwidth, and capacity. Thus, nanophotonics provides an effective solution to the current obstacles that seriously limit the further improvement of modern electronics. Utilizing inorganic/organic nanostructures as photonic materials becomes an ascendant branch of nanophotonics. There is no existing guidance for the design and synthesis of photonic materials and functional devices due to the vast differences between photons and electrons in fundamental physical properties at the moment. Chemists and material scientists, in this respect, contribute enormously to the achievement of novel optical properties with inorganic materials, such as ZnO, CdSe, and noble metal nanostructures, especially gold and silver [2]. During the flourish of their inorganic counterparts, organics are gradually becoming a better choice as nanophotonic materials due to numerous advantages. Organic compounds possess high photoluminescence quantum yields, tunable optical properties, and rapid photoresponses. The excellent flexibility and processability are also big pluses in the construction and assembly of functional photonic devices. Taken together, it is no doubt that organic molecular materials would bring great innovation in the design and fabrication of functional elements toward photonic integrated circuits [3].

For organic compounds, the interactions among molecules, such as hydrogen bonds, van der Waals forces, π–π interactions, and electrostatic forces, are of weak type [4]. These weak intermolecular interactions allow for more facile and mild conditions in the fabrication of crystalline low-dimensional structures through a spontaneous or nonspontaneous assembly process. There have been numerous efforts in the preparation of organic nanostructures through a variety of methods, which can be divided into assembly in the liquid phase, epitaxial

Soft Matter Nanotechnology: From Structure to Function, First Edition.
Edited by Xiaodong Chen and Harald Fuchs.
© 2015 Wiley-VCH Verlag GmbH & Co. KGaA. Published 2015 by Wiley-VCH Verlag GmbH & Co. KGaA.

growth in the vapor phase, and template-based methods [5]. It has been demonstrated that molecular interactions play a crucial role in dominating the assembly characteristics [6]. In general, participation of a single force will induce a one-dimensional (1D) molecular packing along a preferential direction. The simultaneous participation of two or more kinds of interactions would complicate the assembly behavior and nanostructures with various geometries are expected. It is increasingly necessary to summarize the relationship between the intermolecular interactions and the final structural features to further guide the molecular design and construction strategy optimization.

One of the most important reasons why organic nanomaterials have become so attractive in the photonics field is their unique optical properties and light–matter interactions, which are fundamentally different from the inorganic counterparts [7]. The optical properties of assembled molecular nanocrystals depend not only on the properties of molecules constituting them, but also on the morphologies of aggregated products [8]. Aggregation-induced enhanced photoluminescence [9], which arises from the reduced vibration–rotation in the solid state, has been widely reported in various compounds. In addition, those as-prepared nanostructures with regular shapes exhibit remarkable photon confinements, including but not limiting to cavity effect and waveguide behavior. Moreover, the strong coupling between photons and Frenkel-type excitons would generate a new type of quasiparticles, called exciton polaritons (EPs), which can significantly influence the original properties and give rise to a number of new phenomena [10]. The fruitful excited-state processes among different molecules, that is, energy/charge transfer, exciton diffusion, separation, conversion, and recombination [11], could bring much flexibility in the construction of complex photonic elements. Therefore, an in-depth understanding of the relationship between photonic properties and aggregated structures is essential to direct the material design, synthesis, and application.

In this chapter, we mainly concentrate on the relationships among molecules, assembly, structures, and photonic properties, which are divided into three parts (Figure 5.1). We begin with how optofunctional molecules start to assemble under various intermolecular forces (part 2). Then, we put emphasis on the relationship between assembly behavior and final morphologies of the obtained low-dimensional structures, with the aim of fabricating diverse nanostructures through rational control of intermolecular interactions (part 3). In the following part, we will focus on the structural design and corresponding cooperative assembly method of multiple molecules toward complex photonic functions and high performance (part 4). Finally, we summarize the recent contributions as well as challenges in this field and put forward the prospects and directions for future development.

5.2 From Molecules to Assembly

A facile strategy to construct organic low-dimensional structures is essential to further investigate the optofunctions. There are several well-understood methods

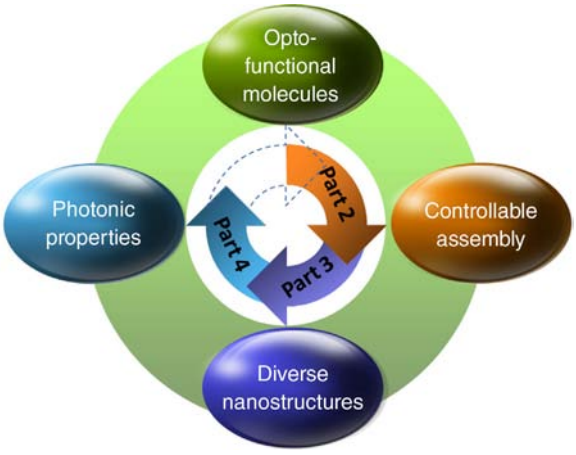

Figure 5.1 Organization of this chapter. Part 2: molecular assembly characteristics, which are determined by intermolecular interactions. Part 3: low-dimensional structures with diverse morphologies through the modulated assembly processes. Part 4: optical properties and photonic applications of the assembled complex structures.

for inorganic materials, which are not suitable for organic materials because of the vicious reaction conditions, such as high pressure, high temperature, and various solvents. Fortunately, some meaningful attempts for synthesizing organic nanostructures have been made in the past few years and assembly has been demonstrated to be a facile and universal route to the acquisition of organic solid materials [12]. This bottom-up method starts from the aggregation of individual molecules and ends up with dynamic balance in the liquid phase or depletion of raw materials in the vapor phase.

Organic molecules could assemble into micro-/nanocrystals on some occasions if the nucleation and crystal growth processes coexist in a system. The tiny aggregations assembled at the initial stage can serve as stable nuclei once they reach a critical size. Then the crystals grow larger and larger until the whole system reaches dynamic equilibrium. The assembly process is fundamentally different from a crystallization process, although the final products of the two processes are all crystals. The main difference is the driving force behind the formation of solids. The crystallization process, which consists of nucleation and crystal growth stages, is driven by supersaturation, while the driving forces in the assembly process come from either the inherent weak intermolecular interactions or the influences from the environment. Here, we elaborate on how these interactions affect the molecular behavior in the assembly process.

5.2.1
Inherent Intermolecular Interactions

Among numerous construction strategies for organic micronanostructures, the most widespread one is assembly in the liquid phase, because of the simplicity,

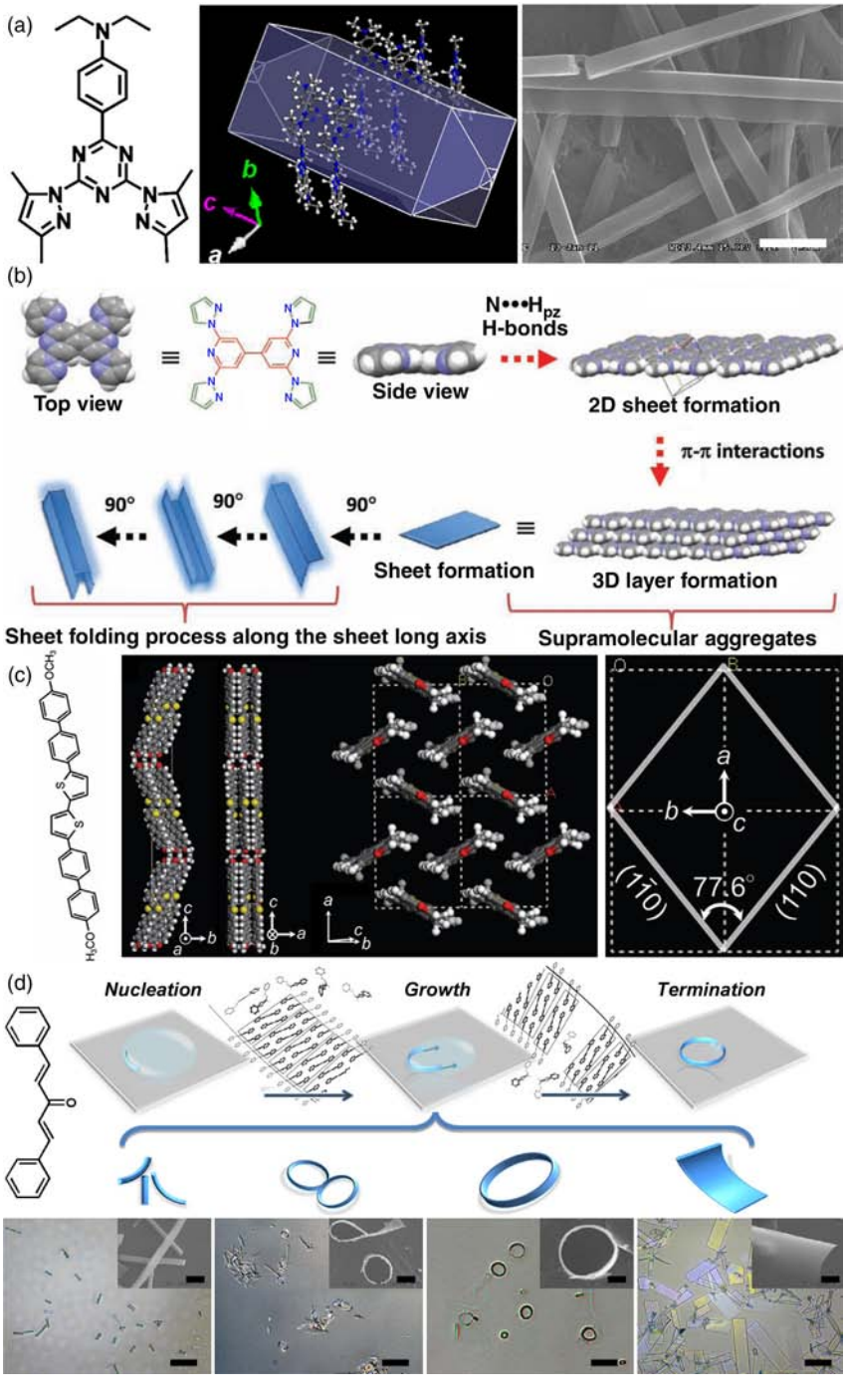
(a)
b
c
a
(b)
Top view
Side view
N•••H$_{pz}$
H-bonds
2D sheet formation
π-π interactions
90°
90°
90°
Sheet formation
3D layer formation
Sheet folding process along the sheet long axis
Supramolecular aggregates
(c)
a
b
c
(1$\bar{1}$0)
77.6°
(110)
(d)
Nucleation
Growth
Termination

flexibility, and easy controllability. By carefully controlling the molecular assembly behavior, we can obtain multiple aggregated materials with regular shapes. For small molecules, the weak interactions among molecules, such as π–π interactions, van der Waals forces, and hydrogen bonds, play a key role in dominating the aggregation behavior. Continuous efforts have been made to explore the relationship between the intermolecular interactions and the pattern modes of molecules in crystalline structures with smooth surfaces and flat end facets.

Figure 5.2 summarizes several typical molecular structures (fibers, tubes, sheets, and rings) fabricated through the assembly behavior of distinct organic molecules. Shown in Figure 5.2a is a representative formation mechanism of the 1D structures, which are assembled from a π-conjugated compound, 2-(*N*,*N*-diethylanilin-4-yl)-4,6-bis(3,5-dimethylpyrazol-1-yl)-1,3,5-triazine (DBPT) [13]. It is indicated in the middle of Figure 5.2a that the DBPT molecule has a preferential packing direction along the *c* crystal axis due to the strong π–π interaction stemming from the middle core. Therefore, DBPT molecules stack one by one along the [001] direction, leading to the formation of wire-like nanostructures. The SEM image displayed in Figure 5.2a (right) further confirms that the 1D structures growing along a single direction are smooth surfaced. The end facets are flat enough to serve as reflectors of high-quality Fabry–Pérot cavities.

Things change if there are more than one kind of intermolecular interactions during the assembly process. Figure 5.2b schematically elucidates the formation mechanism of tubular structures from a novel back-to-back coupled 2,6-dipyrazol-1-ylpyridine compound [14]. As shown in Figure 5.2b, the molecule is near planar (demonstrated by the optimized top-view and side-view images). The hydrogen bond formed by pyrazole ring nitrogen and pyrazole ring proton facilitates a head-to-tail packing mode and thus forms a 1D chain-like structure, which is then closely packed and forms a pseudo-sheet-like structure. These sheet-like structures could aggregate into a 3D multilayered supramolecular structure via intermolecular π–π interactions of the pyridine rings. These supramolecular aggregates are not thermodynamically stable, and an upfolding of 90° along the sheet axis occurs to minimize the surface energy. After a subsequent seaming process, these triple-folded nanosheets formed a rectangular tube-like

Figure 5.2 Formation mechanisms of four representative structures. (a) Nanowire: (left) molecular structure of DBPT; (middle) predicted growth morphology of DBPT crystalline structure; and (right) SEM image of the DBPT nanowires. Scale bar is 2 μm. (b) Schematic elucidation of the possible formation mechanism of tubular structures via supramolecular assembly of 2,6-dipyrazol-1-ylpyridine. (c) Nanosheet: (left) molecular structure of BP2T-OMe; (middle) crystal structures of BP2T-OMe with projections of *bc*-plane, *ac*-plane, and herringbone packing mode along the *c*-axis, respectively; and (right) crystal lattice in the *ab*-plane. (d) Microring: (top) molecular structure of DPPDO and illustration of assembling mechanism of microrings; and (bottom) optical microscopy images of nanowires, small/large rings, and tiles by using DPPDO solutions with different concentrations. Scale bars are 25 μm. Insets show the corresponding SEM images. Scale bars are 2 μm. ((a) Ref. [13], copyright 2011, American Chemical Society; (b) Ref. [14], copyright 2011, Wiley; (c) Ref. [15], copyright 2012, Wiley; (d) Ref. [17], copyright 2013, Wiley.)

structure. The further growth of the tube along the axis was steered by the rapid growth of the tube walls.

Figure 5.2c shows a molecular structure and the stacking pattern in the corresponding low-dimensional crystals with a consequent rhombus shape [15]. This model compound, 5,5′-bis(4′-methoxybiphenyl-4-yl)-2,2′-bithiophene (BP2T-OMe), has a long-chain core of thiophene/phenylene co-oligomer (Figure 5.2c, left), which has been used extensively as gain medium for lasing. In the middle of Figure 5.2c, it is indicated that the molecules are tilted against the *ab*-plane, which is governed by the interactions between peripheral methoxy groups. The molecular axes are alternately declined in the opposite direction to the *c*-axis in the stacked molecular layers because of the zigzag molecular shape. When projected along the molecular axis in one molecular layer in parallel to the *ab*-plane, a classic herringbone packing is clearly observed. The π-stacking and interactions between neighboring methoxy groups are responsible for the two-dimensional shape, because hydrogen atoms on the molecular terminals do not contribute to the stabilization of an orthorhombic form [16]. The angle between the (110) and $(1\bar{1}0)$ faces of the crystal is determined to be 77.6°, which is close to the edge angle of the rhombus shape of the sheet.

Recently, Zhao's group succeeded in a controllable construction of ring-shaped structures with an organic compound named 1,5-diphenyl-1,4-pentadien-3-one (DPPDO) [17]. Such a molecule, whose structure is displayed in Figure 5.2d, exhibits a good tolerance for structural distortion due to the rearrangement of molecules in the loose crystal lattice. The molecular planes are perpendicular to the *c*-axis and the distance between adjacent molecules along the *c*-axis is a bit large, affording a buffer space for the slight movement of DPPDO molecules. As a result, the assembled DPPDO 1D structures are of remarkable flexibility, implying bendable characteristics in the preferential growth directions. Therefore, it is likely to achieve microrings from the assembly of DPPDO molecules, as long as an appropriate driving force could be applied for the circular growth during the assembly process.

The crystalline microrings were fabricated with the action of the liquid tension during the assembly process. As shown in Figure 5.2d, the DPPDO molecules concentrate preferentially first at the contact line between microsized droplet and substrate, where the solvent evaporated faster than that in other areas. The solution droplet was therefore confined within the inner surface, acting as a circular template for the assembly. Along with the enlargement of DPPDO segments, molecular packing starts to bend, which is induced by the force of liquid tension at the contact line. With the further evaporation of solvent, the segments gradually grow into a curved belt. The formation of the rings heavily depends on the amount of DPPDO units in the microdroplets (Figure 5.2d, bottom). If there are no sufficient molecules, only short rods would appear. With the increase of DPPDO amount, the products gradually develop into incomplete and perfect microrings. However, only large tiles emerge if excess DPPDO were put in a droplet, because of the huge mechanical resistance that needs to be overcome for the wide tiles to bend. From this result, we can infer that although intermolecular

forces dominate the assembly behavior and thus the final morphology, other influences, such as the amount of DPPDO [18], should not be ignored.

5.2.2 Influences of External Factors

Except for inherent intermolecular forces, some other external conditions, including solvent, humidity [19], surface tension, temperature [20], aging time [21], and ultrasonic action [22], also play a role in determining the assembly behavior of molecules. For example, a highly humid condition would be crucial to the formation of ring-shaped structures for thiacyanine derivatives [19]. Zhang *et al.* reported that by changing the process temperature, three kinds of single-crystal nanostructures, for example, nanoribbons, nanotubes, and nanowires, can be controllably prepared with a single intramolecular charge transfer organic compound [20].

5.2.2.1 Solvent Effect in Assembly

Figure 5.3 illustrates an example of solvent effect on the assembly and final products with distinct morphologies, for example, solid rods and hollow tubes, respectively. Both the structures were formed by assembly in the liquid phase with the same compound [21]. Briefly, dilute 9,10-bis(phenylethynyl)anthracene (BPEA) solution was injected into boiling water under vigorous agitation and then cooled to room temperature. The assembled products are rod-like crystals, as proved by the SEM image in Figure 5.3a. The magnified image of a single rod tip shown in the inset indicates that the end face is relatively flat. If the boiling system was kept refluxed for a period before cooling, the assembled products would be perfectly hollow tubes (Figure 5.3b), which were further confirmed by the TEM image (Figure 5.3c). The preferential growth directions of the two distinct structures are the same (Figure 5.3c, inset), revealing some inherent connections. The reason why reflux enables the formation of hollow structure was explored through a variation of reflux time. It is the etching of BPEA molecules by the small amount of ethanol (the good solvent) during the reflux period that resulted in the formation of the hollow tubular structures [23].

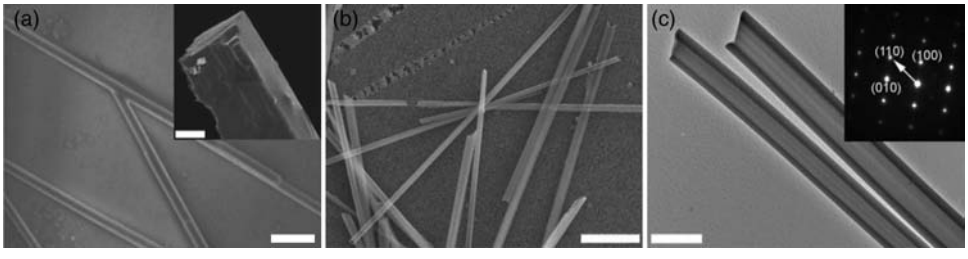

Figure 5.3 Solvent etching effect on the assembly. (a) SEM image of the BPEA microrods prepared with a regular liquid-phase assembly. Scale bar is 5 μm. *Inset*: SEM image of a single rod tip. (b) SEM image of BPEA microtubes prepared through an assembly process under reflux. Scale bar is 10 μm. (c) TEM image of the typical BPEA microtubes. Scale bar is 2 μm. (*Inset*: SAED pattern. Copyright 2008, Wiley.)

5.2.2.2 Site-Selected Assembly on Specific Substrates

For assembly in the liquid phase, the solvent is especially significant mainly because of the fact that some other factors come into play through it, such as temperature, solubility, aging time, and surface tension. In contrast, the most important factor for assembly in the vapor phase is the parameters of vaporized organic molecules. The supersaturation degree of the vaporized molecules has been demonstrated to be the key factor in deciding the morphology and monodispersity of aggregates [24]. Maintaining the vapor saturation at an appropriate level will facilitate the assembly of most organic compounds into uniform low-dimensional structures. Thus, it is increasingly important to be able to control such a parameter.

It was reported that the introduction of adsorbent would improve the quality remarkably in vapor-phase deposition [25]. The adsorbents, which can be neutral aluminum oxide or silica gel, are extremely effective in controlling the degree of supersaturation. The mechanism is considered to be associated with an adsorption–desorption equilibrium between the adsorbents and the organic sources. A variety of organic nanocrystals have been fabricated with this improved method. Taking tris(8-hydroxyquinoline)aluminum (Alq_3) as an example, Figure 5.4a illustrates a typical assembly process in the gas phase. The material source, which is a mixture of Alq_3 and adsorbent, is heated to the deposition temperature with a furnace. The sublimed Alq_3 vapor with proper flux translates

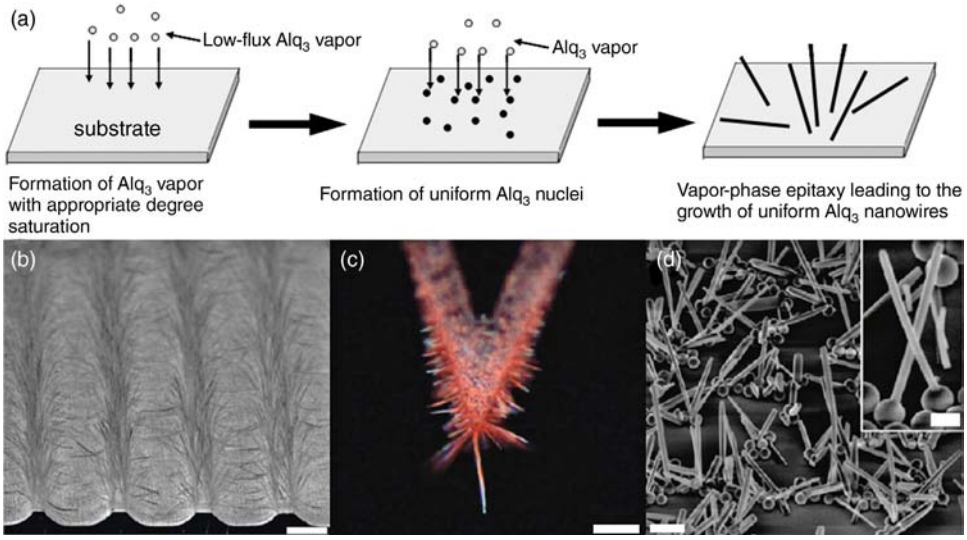

Figure 5.4 Substrate effect on the assembly of organic molecules in the vapor phase. (a) Growth mechanism of Alq_3 nanowires with the assistance of adsorbents to improve the uniformity and crystallinity. (b) Patterned growth of DAAQ nanowire arrays on silicon wafers with periodic ridge–groove patterns. Scale bar is 25 μm. (c) Optical microscopy image of the DAAQ nanowires grown at an AFM tip. Scale bar is 10 μm. (d) SEM image of the DAAQ nanowires grown on silica spheres. Inset is the magnified image. Scale bars are 2 μm. ((a) Copyright 2006, Wiley; (b–d) copyright 2010, American Chemical Society.)

into small Alq_3 crystal nuclei with high uniformity on the substrates. Then subsequent Alq_3 molecules adsorbed onto the nuclei through intermolecular interactions and grew into uniform 1D structures.

The acquisition of nanowire arrays has been actively pursued because of the improved properties for wide applications, such as efficient solar cells, high-capacity batteries, and light-emitting diodes. Previous works on array materials mostly concentrated on inorganic semiconductors [26] or materials fabricated through various templates [27,28]. Since organic materials have been widely used in the photoelectric area, it is necessary to acquire crystalline organic nanowire arrays. Huang and coworkers reported a direct fabrication method of vertically aligned organic nanowire arrays [29]. It was found that 1,5-diaminoanthraquinone (DAAQ) tends to preferably nucleate and grow faster on sites with high surface energy. This site-selected growth enables a patterned growth on modified substrates. Figure 5.4b is the tilted view SEM image of DAAQ arrays grown on a silicon plate with alternating ridge edges and grooves. Here, DAAQ molecules selectively nucleate and grow on ridge edges where the surface energy is much higher than that of grooves. For the same reason, DAAQ molecules could also grow on AFM tips (Figure 5.4c) with a much longer wire near the very end tip, which possesses the highest surface energy. This reminds us that introducing extra sites with high surface energy should be an effective way to control the distribution of the obtained nanostructures. It has been proved that the size of growth site affects the number and orientation of DAAQ nanowires. As demonstrated in Figure 5.4d, only one nanowire grew on each silica sphere with a proper diameter of 520 nm. The ease of the oriented vertical growth and modulation provides convenience for the fabrication of complex structures as well as direct integration of nanowires into devices.

5.3
From Assembly to Structures

Organic nanostructures have become so attractive in recent decades mainly because of their unique optical and electronic properties. To our knowledge, the optical performances of organic nanostructures are determined by both the intrinsic properties of molecules constituting them and the optical confinement arising from the structural features. Organic aggregates assembled from small molecules are usually crystals with regular geometric shape, where the ordered molecular arrangements present good photon confinement. From the previous section, we know that the molecular assembly behaviors directly determine the final structures of tiny crystals. That is to say, the acquisition of distinct structures can be reasonably expected through a fine control of the assembly process. In this section, we will discuss the achievements of nanomaterials with specific structures either through rational molecular design or through construction strategy selection.

5.3.1 Structure Control through Intermolecular Interactions

We know that molecules would aggregate into various low-dimensional structures if appropriate forces were introduced during the assembly process. Since the optical properties are strongly structure dependent, a controllable synthesis is of particular significance. In most cases, aromatic molecules could assemble into 1D structures through strong π-stacking if there are no other intermolecular interactions. Modifying molecular structure by tailoring the constituent groups may introduce extra forces, causing different preferential packing modes, such as direction, planarity, and steric hindrance effect. Thus, the rational design of molecular components with different intermolecular recognition patterns would be promising for the acquisition of nanostructures with predefined morphologies, which can manipulate photons in specific ways.

5.3.1.1 Controlling the Structures via Molecular Design

Very recently, Zhao's group constructed 1D and 2D nanoarchitectures through assembly by varying the molecular components, affording a guideline to the function-guided molecular design and morphology control (Figure 5.5) [30]. The only difference between 2-acetyl-6-dimethylaminonaphthalene (ADN, Figure 5.5a) and 2-acetyl-6-methylaminonaphthalene (AMN, Figure 5.5e) is the peripheric substituents on the naphthalene core. The secondary amine in AMN could afford less steric repulsion with neighboring molecules and an extra hydrogen bonding site, hindering the 1D packing. It is predicted from the thermodynamical perspective that the stable morphology for ADN is wire-like, while AMN molecules would be

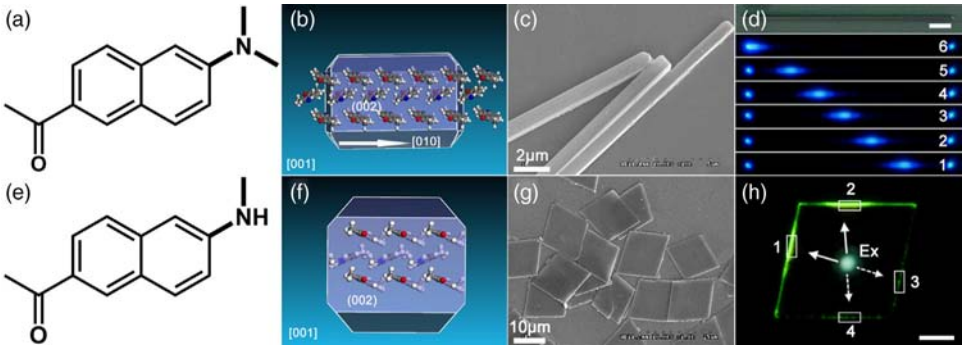

Figure 5.5 Assembled structures with 1D and 2D features through molecular design. (a and e) Molecular structures of ADN and AMN compounds, respectively. (b and f) Predicted growth morphologies based on the attachment energies of ADN and AMN molecules, respectively. (c and g) SEM images of 1D nanowires aggregated from ADN and 2D rhombic plates from AMN molecules, respectively. (d and h) Distinct waveguide behaviors of 1D and 2D structures, respectively. Scale bars in (d) and (h) are 5 and 10 μm, respectively. (Copyright 2013, Wiley.)

arranged in a slip-stack mode to form sheet-like structure (Figure 5.5b and f, respectively).

The 1D growth of ADN (Figure 5.5c) was determined to be along [010] direction, which can be attributed to the π–π interactions. These wires can serve as active waveguides where the emitted light is confined within the nanowire and propagates along the axis in two predominant directions (Figure 5.5d). There is no obvious light loss from the light intensities for positions 1–6 (labeled in Figure 5.5d) with the increase of propagation length, indicating a low-loss transmission. Similarly, the two preferential growth directions of the 2D rhombic sheets (Figure 5.5g) are [100] and [010], which are associated with the π–π interaction and hydrogen bond interactions, respectively. When a focused laser beam irradiated the center of the rhombus plate, the neighboring two outcoupled edges (marked with 1 and 2, Figure 5.5h) have large, bright fluorescence emissions, which show significant contrast with the small, obscure outcouplings at the opposite edges (3 and 4). The remarkable intensity difference between edges of an acute angle implies an asymmetric light propagation, which may play a fundamental role in creating new types of devices.

For organic compounds, not only the differences of substituent groups [19,31], but also their positions may significantly influence the major driving forces in the assembly process, and thus the structures of final products [32]. It has been proved that three isometric molecules of bis(iminopyrrole)benzene could assemble into well-defined spheres, wires, and cubes, respectively, although the intermolecular forces are the same. Different interactions for aggregate stacking at the supramolecular level caused by the isomeric molecular structures are most likely responsible for the different morphological evolution.

5.3.1.2 Structures Obtained from the Synergistic Assembly of Different Compounds

Intermolecular interactions between different compounds can be utilized to fabricate multicomponent structures through their cooperative assembly [33]. In general, the selected compounds constitute a donor–acceptor pair with efficient energy transfer, where a small amount of energy acceptor would quench the donor emission heavily. The energy transfer process through either dipole–dipole interaction or electron exchange would be very effective for organic solid systems due to the reduced intermolecular distance. Benefiting from the fruitful excited-state dynamics, the doped structures could not only maintain the advantages of each component, but also provide novel optical performances, for example, tunable color emission or white light emission [34]. Therefore, exploration of construction strategy to binary systems has a far-reaching consequence to the overall manipulation of photon parameters.

Figure 5.6 presents two typical 1D binary structures obtained by the co-assembly of different molecules. The well-defined nanorods shown in Figure 5.6a were prepared through the adsorbent-assisted epitaxial growth method with two dyes, a blue light emitter (1,3,5-triphenyl-2-pyrazoline, TPP) and an orange light emitter (rubrene). The dopant was determined to be uniformly distributed in the TPP host, ensuring an efficient Förster resonant energy transfer (FRET) process.

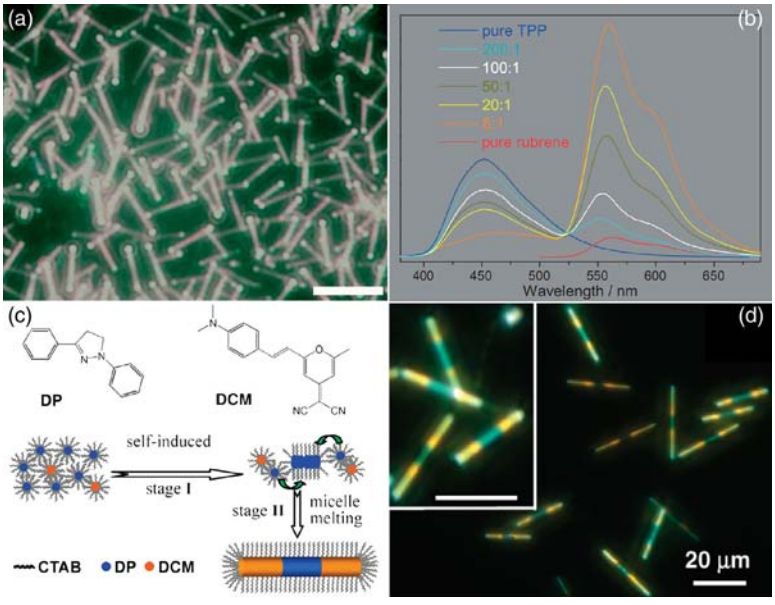

Figure 5.6 Composite structures fabricated from the synergistic assembly of different molecules. (a) PL microscopy image of TPP/rubrene nanorods with controllable doping ratios. Scale bar is 5 μm. (b) Emission spectra of the TPP/rubrene nanostructures with different doping contents. (c) Molecular structures of DP and DCM as well as the illustration for formation mechanism of the gradiently doped microrods. (d) PL microscopy image of the microrods under UV illumination. ((a and b) Copyright 2008, Wiley; (c and d) copyright 2010, American Chemical Society.)

The emission color varies significantly with the rubrene doping content, which was modulated by changing the molar ratio of the source materials (Figure 5.6b). At first, there was only one characteristic fluorescence band for pure TPP nanostructures. With the increase of rubrene amount, the emission of TPP was quenched gradually, while the emission corresponding to the rubrene rose up rapidly. When the TPP/rubrene molar ratio was fixed at 100:1, a stable white light emission can be reached from these 1D nanostructures.

Yao and coworkers reported a supramolecular synthesis of triblock microrods constituted with 1,3-diphenyl-2-pyroline (DP) and 4-(dicyanomethylene)-2-methyl-6-(*p*-dimethylaminostyryl)-4*H*-yran (DCM) [35], as illustrated in Figure 5.6c. With the assistance of cetyltrimethylammonium bromide (CTAB) micelles, the DCM molecules could selectively deposit at both ends of the DP rods. During the synergetic assembly process, DP molecules first dissolved into the hydrophobic core of the spherical CTAB micelles due to the solubilization effect (stage I). The dissolution of DP molecules helps in the formation of rod-like micelles that in turn act as templates directing the primary growth of DP molecules. Finally, DCM molecules started to codeposit with DP molecules, generating the triblock microrods (Figure 5.6d). Although these microrods exhibit microarea heterogeneity, they show macroscopic high-quality white light emission properties.

5.3.2
Structure Modulation through External Factors

From the above discussion, we know that the environment plays a complementary role in the assembly process. Utilizing this point, we could intervene in the molecular assembly behavior by adjusting ambients on the basis of a clear aggregation picture. For example, both the rod and wire structures can be obtained with the same *fac*-tris(2-phenylpyridine)iridium ($Ir(ppy)_3$) compound, but using different methods. The assembled structures from solvent exchange and solvent evaporation methods are of different crystalline forms [36]. Also, reversible nanostructure conversion from nanospheres to nanorods and nanosheets has also been realized [37].

5.3.2.1 Structures versus Aging Time

Recently, a partly reversible shape shifting of 1,4-bis(1,2′:6′,1″-bis(3-butyl-1*H*-3,4,5-triazolyl)pyridin-4′-yl)benzene nanostructures was reported by Chandrasekar's group, as shown in Figure 5.7 [38]. The molecule has a rod-shaped arrange-

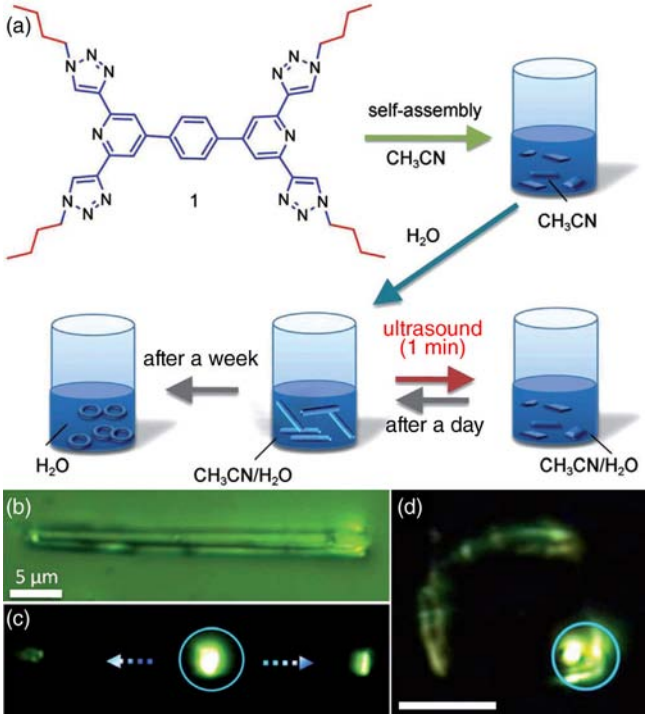

Figure 5.7 Various assembled nanostructures and corresponding optical properties obtained with different assembly conditions. (a) Sketch map of the formation of 2D rectangular plates, 1D nanotubes, and 0D nanorings of the compound under different conditions. (b and c) Optical bright-field and photoluminescence microscopy images of an identical microtube, respectively. (d) Photoluminescence microscopy image of a single nanosheet with a laser excitation at the corner. (Copyright 2012, Wiley.)

ment of three aromatic rings in the center (Figure 5.7a), which ensures a nice molecular planarity. The nitrogen atom in triazole ring (N_2) would participate in two hydrogen bond interactions with phenyl ring protons, playing a major role in the supramolecular ordering. Homogeneous rectangular sheets are easily achieved through an assembly process in solution. Those microsized plates could switch into tubes via a rolling mechanism in the presence of water, while sonication could induce a reverse transformation of the tubes back into plates. The nanorings were obtained from the tube solution after a week and the transformation process is irreversible.

The absence of any external interference during the whole structural evolution process suggests that the critical activation energy needed to overcome the intermolecular binding forces is very low. For this case, the driving force behind the structural deformation was ascribed to the hydrophobic surface effect, which propels these sheets to curve to avoid the exposure to water. Anisotropy optical waveguide was observed with the excitation of a focused laser beam, demonstrating a possibility of switching the wave guiding behavior through light propagating direction in both 1D (Figure 5.7b and c) and 2D (Figure 5.7d) structures. This work announces again that various optical performances for different application can be achieved even from the same compound as long as an appropriate assembly condition is predesigned. Before that, a careful analysis of the relationship between intermolecular/environmental interactions and structures is indispensable to choose proper assembly strategies.

5.3.2.2 Heterostructures through Site-Specific Epitaxial Growth

The site-specific nucleation characteristics of organic molecules are promising in fabricating some complex structures, for example, organic–metal nanowire heterojunctions, which were realized recently by our group via the vapor deposition of organic compounds on silicon substrates with predispersed silver nanowires (Figure 5.8) [39]. Figure 5.8a is the SEM image of crystalline silver nanowires with convex vertices, which ensure an overwhelming superiority in attracting vaporized BPEA molecules. During the deposition process, the sharp wire tips serve as nuclei centers for the condensation of BPEA vapor. Finally, BPEA molecules nucleated specifically adjacent to the tips of the silver wires to form heterojunctions (Figure 5.8b), which is confirmed by the TEM image of a single BPEA–silver nanowire junction area (Figure 5.8c).

Shown in Figure 5.8d and e are the bright-field and photoluminescence microscopy images of an identical organic–silver nanowire heterojunction. The great contrast in Figure 5.8d reveals that the two wires are of different quality. Both tips of the BPEA wire and the joint point emit bright yellow light under an excitation of a focused laser beam, which is a characteristic of active waveguide. The red emission, emitted from the end of silver nanowire, can be modulated through the polarization of the incident beam, which is attributed to the direct exciton polariton–plasmon coupling. The distinct characteristic of EPs in organic nanowires supplies a new idea to realize logic operations with an individual heterojunction. This facile two-step growth strategy provides a remarkable

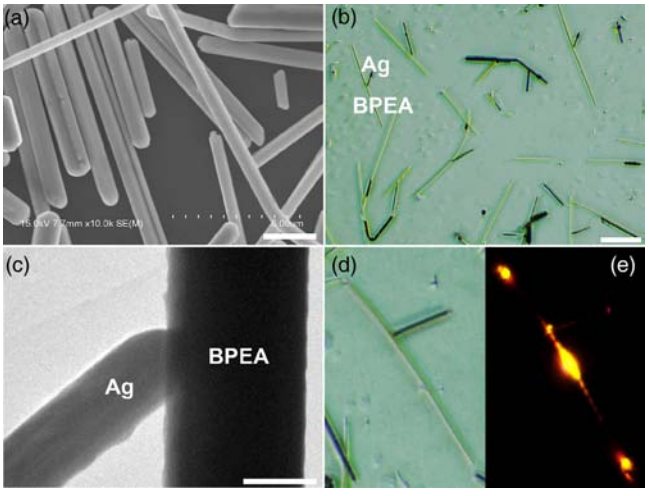

Figure 5.8 Preparation of organic–metal nanowire heterojunctions through substrate modification. (a) SEM image of the silver nanowires with convex tips. Scale bar is 2 μm. (b) Optical microscopy image of the BPEA–silver heterojunctions. Scale bar is 20 μm. (c) TEM image of the junction area. Scale bar is 200 nm. (d and e) Optical bright-field and PL microscopy images of an identical junction, respectively. (Copyright 2012, Wiley.)

convenience for incorporating plasmonic modules as practical components into high-capacity photonic circuits.

5.4
From Structures to Photonic Properties

Low-dimensional structures constructed from single kind of compounds offer an ideal model to study the assembly characteristics as well as structure-related light confinement and electronic properties [40]. Now we have reached a preliminary comprehension in the relationships among molecule, assembly, and structure from the previous two sections. The abundant interactions among different materials, such as energy/charge transfer, exciton migration and conversion, and EP–SPP coupling, have a fair chance of generating a series of novel properties in complex structures. An ingenious utilization of these new mechanisms would be of great significance to the realization of photonic devices with desired functions [11]. Thus, in this section, we will focus on the optical properties and corresponding applications of three representative complex structures assembled from organic molecules.

5.4.1
Nanowire Heterojunctions

In comparison with uniformly doped structures, heterostructured materials with a clear interface are much more flexible in the manipulation of photons at the

micro-/nanoscale. Some innovative effects could be utilized to finely tune the light–matter interactions and thus bring out meaningful optical properties. For example, multiple segmented nanostructures show broad multifunctionality in photonic applications, including nanobarcodes [35], p–n junctions [41], and multiluminescent light sources. However, these phase-separated low-dimensional structures were mainly prepared via hard template or electrochemical deposition techniques, with a great weakness of photoelectric properties due to the amorphous structures. Along with our knowledge on the controllable assembly, heterostructures could also be prepared via modified assembly [42].

5.4.1.1 Dendritic Heterostructures as Optical Routers

Organic dendritic structures have been actively investigated due to their potential applications in one-to-many, many-to-one, and many-to-many photonic devices. Inspired by the fact that vaporized organic molecules tend to nucleate preferentially and grow more rapidly on sites with smaller curvature radii or higher surface energies [29], Zhao and coworkers proposed a two-step deposition method to create organic wire-on-wire structures (Figure 5.9a) [43]. In a typical synthesis, assembled crystalline Alq_3 microwires (step 1) with hexagonal cross sections (Figure 5.9b) were used as nucleation centers for the vertical epitaxial growth of DAAQ molecules (step 2). DAAQ molecules concentrate selectively on the Alq_3 microwires to form isolated clusters, seeding subsequent molecular deposition to form the final vertical nanowire branches. Such a growth mechanism has been testified by the SEM images of different growth stages (Figure 5.9c–e). Both the branch density and length can be precisely controlled by deposition time and temperature, respectively, illustrating the versatility and universality of the fabrication method. The green emission from Alq_3 trunk and red emission from DAAQ branches are clearly observed in corresponding positions (Figure 5.9f), verifying the phase-separated component distribution and existence of clear interfaces.

The obtained heterostructures function as optical routers with many output channels so that the guided light can be output simultaneously from the trunk tips and each branch under an excitation (Figure 5.9g). The spatially resolved PL spectra (Figure 5.9h) from different branches demonstrate the propagation length-dependent outputs as well as color changes (inset). In comparison with the PL of Alq_3 (curve I in Figure 5.9h), the spectra taken locally from the trunk tip (curve V) show a red shift due to the variation in the energy transfer process. The other three curves are all superpositions of the green and red emissions from the two compositions, indicating the simultaneous occurrence of efficient FRET processes and the direct guidance of Alq_3 emission in DAAQ branches at the interfaces. The decreased fluorescence lifetime of Alq_3 emission at different positions (Figure 5.9h) further confirmed the different energy transfer efficiency.

5.4.1.2 Nanowire p–n Junctions as Photoelectric Transducers

If both the nucleation spots and the growth direction can be simultaneously controlled with a high accuracy, where only one wire grows vertically on the

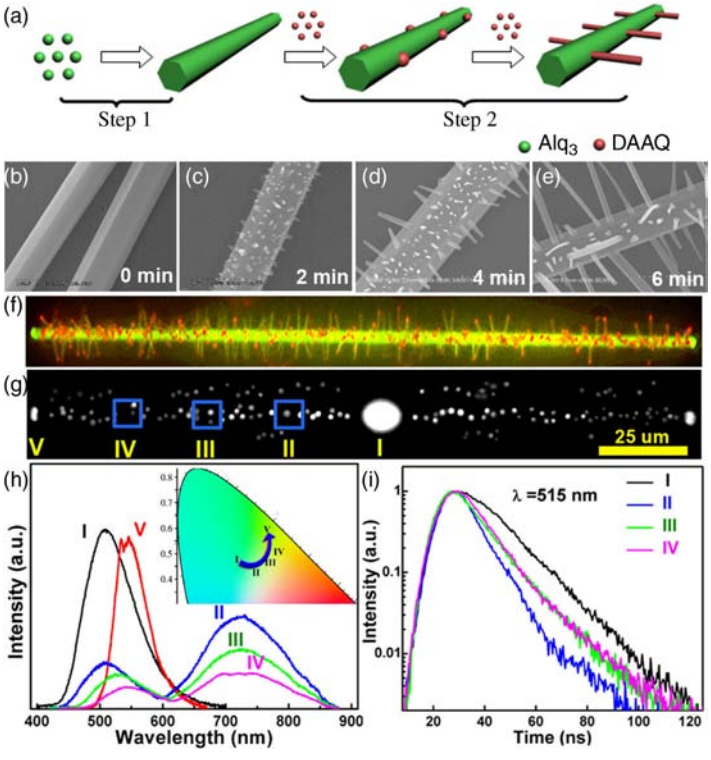

Figure 5.9 Growth processes and photonic properties of the dendritic organic–metal nanowire heterojunctions. (a) Schematic illustration of the growth mechanism. Step 1: Alq_3 microwire prepared through assembly in the liquid phase. Step 2: site-specific nucleation and epitaxial growth of DAAQ molecules on the Alq_3 microwires. (b–e) SEM images of different growth stages of DAAQ in step 2. (f) PL microscopy image of a single nanowire heterojunction under the illumination of unfocused UV light. (g) PL microscopy image of the heterostructure under the excitation of a focused laser beam. (h) Spatially resolved photoluminescence spectra of the excited spot (I), output signals from the DAAQ branches (II–IV), and the Alq_3 tip (V) labeled in (g). (i) Photoluminescence decay profiles of Alq_3 emissions at different propagation lengths. (Copyright 2012, American Chemical Society.)

predispersed wire, crystalline heterojunctions, even arrays, would be available [44]. The preparation method might be a two-step process as previously discussed or just a one-step process, for example, epitaxial growth via vapor-phase codeposition, as illustrated in Figure 5.10a [41]. Here, two compounds with similar molecular structures, the p-type material (copper phthalocyanine, CuPc) and the n-type material (5,10,15,20-tetra(4-pyridyl)porphyrin, H_2TPyP), were selected for the synthesis of coaxial p–n junction nanowire arrays. Both compounds were put in a tube furnace at different positions to be coevaporated with a varied evaporation rate. During the deposition process, H_2TPyP forms vertically aligned hollow structures first, which provide nucleation sites for

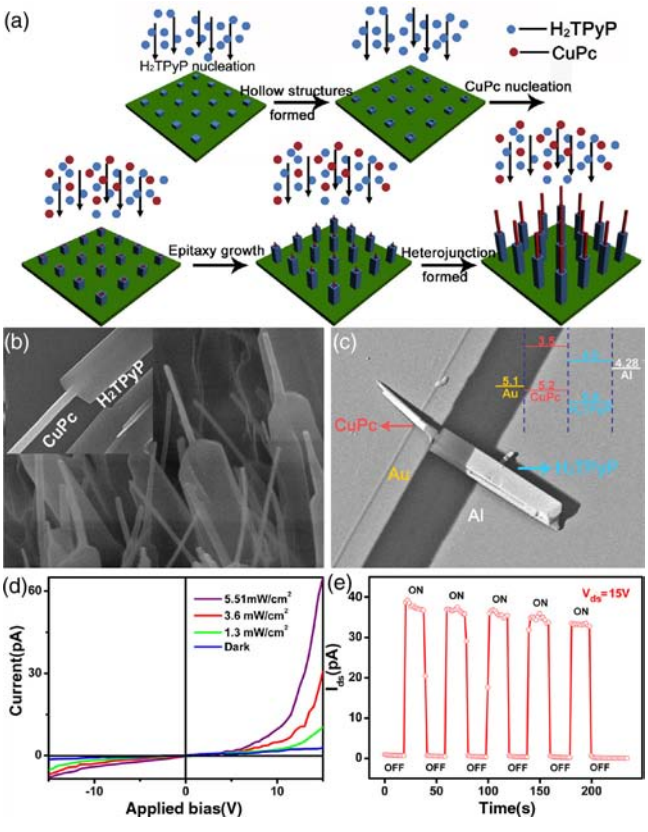

Figure 5.10 Formation and photoelectric properties of the coaxial organic p–n heterojunctions. (a) Schematic illustration of the assembly processes of the CuPc–H_2TPyP p–n junction nanowire arrays. (b) SEM image of the as-prepared nanowire junctions. Scale bar is 1 μm. Inset shows a single heterojunction. (c) SEM image of a photoelectric device based on a single junction. Inset shows the energy level diagram of the device. (d) Current–voltage (*I*–*V*) curves of the device shown in (c). (e) Photoswitching characteristics of the p–n junction device. (Copyright 2012, Wiley.)

subsequent CuPc vapor concentration. Then, the two molecules codeposited for some time to form the heterojunction nanowire arrays (Figure 5.10b).

The strong π–π interactions between the two planar compounds ensure good connections at the junction area that endow each coaxial heterojunction nanowire with excellent photoelectric properties. Shown in Figure 5.10c is a single device with the prepared p–n junction. Such a device acts as a good photoelectric transducer, as depicted in Figure 5.10d and e. The repeatable photocurrent under the light illumination indicates a reversible and stable response to external illumination. The large energy difference between the lowest unoccupied molecular orbital of H_2TPyP and the highest occupied molecular orbital of CuPc at the heterointerface enables a great opportunity for the further

improvement of device efficiency. Commonly, the larger the wire diameters, the higher the device efficiency. Owing to the unique cable-type structure and the large interfacial gap, the single-junction device shows better optoelectronic conversion performance than single-component nanowires and thin film sandwiched devices, which can be applied as highly sensitive photoelectrical transducers in nanoscale photonic circuits.

5.4.2 Doped Nanostructures

The signal sources for an integrated photonic circuit might be a nanolaser with a narrow linewidth or broadband emissions, and even white light, since they provide more possibilities in novel optical signal processing. Doping is a general technique in organic materials to obtain color-tunable emissions due to the efficient energy transfer process. However, the emission colors of the doped structures are usually not stable because of slight acceptor content variation caused by external stimuli. Therefore, developing an intelligent mechanism that can adjust the output automatically, regardless of doping ratio and environmental variation, is necessary and challenging.

5.4.2.1 Uniformly Doped Structures

The combination of FRET downconversion and triplet–triplet energy transfer (TTET) upconversion in an organic system is supposed to fulfill the requirement. Zhao and coworkers fabricated uniform 1D nanostructures with 9,10-diphenylanthracene (DPA) and iridium(III) bis(2-phenylbenzothiozolato-$N,C^{2'}$) acetylacetonate ($(BT)_2Ir(acac)$) through assembly [45]. In these composite nanowires, the bidirectional energy transfer, that is, the FRET from DPA to $(BT)_2Ir(acac)$ and the reverse TTET from $(BT)_2Ir(acac)$ to DPA coexist, causing the energy fluctuations between the singlet and triplet states during the light propagation. The excitons can fluctuate between the blue emission of DPA and the orange emission of $(BT)_2Ir(acac)$ in the binary nanowire. The color ratios of two outcoupling colors from either low- or high-doped wires can reach the same value after the light transmission over a certain distance (Figure 5.11a), resulting in a self-modulated white light outcoupling at wire tips. Such an optical waveguide behaves like a regulator that converts different input colors into a standard output, as displayed in Figure 5.11b. These results provide a comprehensive understanding of exciton polariton conversion in active waveguiding and effective strategies for developing novel multicomponent waveguide building blocks.

Optical switcher is indispensable to perform some ordinary functions in photonic signal processing. The achievement of ON/OFF state for photons is not an easy thing because external activities can hardly intervene in the behavior of photons. Fortunately, various light–matter interactions as well as optical confinement in different tiny structures could be used to solve the problem. Organic molecules, which were endowed with diverse photoresponses, could be conveniently utilized to realize specific functions. For example, photochromism [46], a

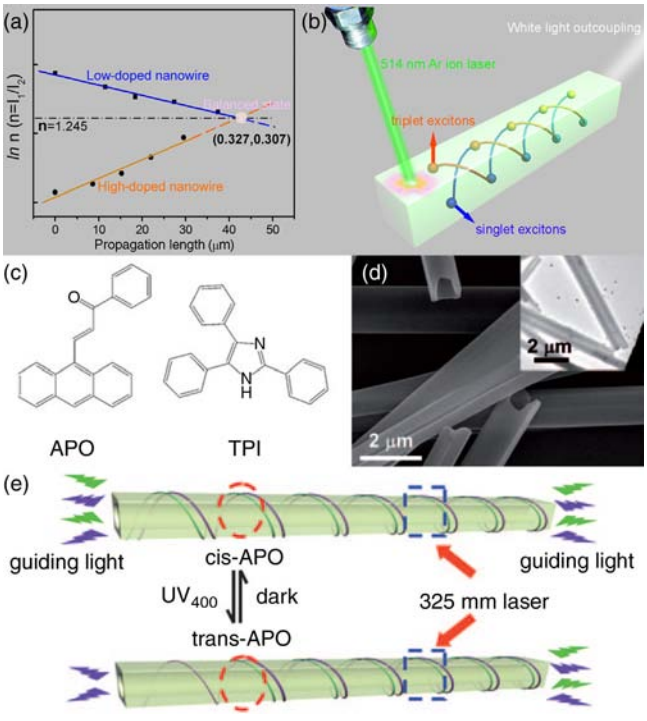

Figure 5.11 Fabrication of uniformly doped structures for light sources with tunable emission colors. (a) The exponential relationship between the contribution ratio of donor to acceptor emission, *n*, and the propagation length in the low- and high-doped nanowires. (b) Schematic illustration of the mechanism for the self-modulated white light outcoupled emission. (c) Molecular structures of APO and TPI. (d) SEM and TEM (inset) images of the 1D doped tubular structures. (e) The principle of the microtubes as optical waveguide switch. The circled areas represent the photoisomerization regions induced by UV irradiation. The squares indicate the excited spots for waveguide measurement. ((a and b) Copyright 2011, Wiley; (c and e) copyright 2011, Wiley.)

reversible change in absorption band governed by the light irradiation, can be applied for the construction of waveguide switcher [47]. Figure 5.11c presents two molecular structures: a photochromic molecule 3-(anthracen-10-yl)-1-phenylpro-2-en-1-one (APO) and 2,4,5-triphenylimidazole (TPI). Homogeneous tubular structures (Figure 5.11d) can be obtained through the synergetic assembly of these two model compounds mediated by hydrogen bonding.

When excited with a focused laser at the squared area (Figure 5.11e), the 1D tube would emit intense fluorescence and self-guide to both tips. After the illumination of 400 nm beam (UV_{400}), the guided light from the left tip decreased dramatically while the emission with a peak of 540 nm disappeared completely. Meanwhile, there is no obvious change in the outcouplings from the right tip before and after the UV irradiation. That is to say, selective switching of the waveguide had been successfully achieved in such a binary structure. The

outcoupled light can be turned on again by keeping the sample in the dark. This switching behavior can be reversibly switched over many cycles without any fatigue, demonstrating a good repeatability and reliability as practical photonic devices. This work also enlightens a way to control the waveguide behavior through the particular properties of molecules.

5.4.2.2 Gradiently Doped Structures

Precise design and fabrication of chemical heterogeneous structures is another good alternative to obtain specific photonic functions. Benefiting from the flexible synthesis through cooperative assembly, the spatial excitonic emission during the light propagation path could be finely engineered through the donor–acceptor energy transfer in organic heterogeneous composites. A template-free method for heterostructures with tunable compositions in the axial direction was developed by Zhao and coworkers [48]. The axial segments were acquired through a proper control of intermolecular interactions between the host and the guest, TPI was selected as the host material, and two compounds – a sphere-like organometallic complex $(BT)_2Ir(acac)$ and a planar molecule BPEA – were selected as typical guest materials. In the assembly process (Figure 5.12a), TPI molecules quickly aggregate into short rod-like hollow structures and then the guest molecules start to enter into the TPI host matrix subsequently. The major difference between the two molecules lies in the host–guest interaction strength, that is, the π–π interaction in the BPEA–TPI pair is much stronger than the van der Waals force in the $(BT)_2Ir(acac)$—TPI pair. Such a divergence results in the axially distinct distribution of the two dopants.

For $(BT)_2Ir(acac)$, the great mismatch with TPI in molecular planarity brings a large steric hindrance, which terminates the further growth of TPI molecules. Therefore, the final products were characterized as three blocks, where the doped components are distributed mostly in both ends (Figure 5.12b). Comparatively, the nice similarity in molecular structures between BPEA and TPI molecules ensures a better molecular compatibility, which allows for the continuous packing of TPI molecules. The consumption of BPEA ends up its aggregation on the TPI host, and then the growth of TPI restarts and becomes predominant. These processes took place repeatedly until the depletion of molecules. The alternant accumulation of TPI and BPEA molecules resulted in the multiblock structures with tunable colors (Figure 5.12c).

This cooperative assembly strategy is universal, which can be generalized and expanded to achieve some complex structures toward practical functions, such as full-color emission in a single tube [14] or triode for signal processing [41,49]. Soon afterward, 3-(2-benzothiazoly)-7-diethylaminocoumarin (coumarin 6) was adopted as the guest compound to acquire nanostructures with distensible color tunability on the basis of the above results. Besides the intrinsic green emission from monomer, coumarin 6 also emits red fluorescence from the charge transfer state in aggregates, as shown in Figure 5.12d. Therefore, red–green–blue full colors in an individual luminescent structure would be accomplished with the TPI–coumarin 6 pair via controllable doping in the assembly process.

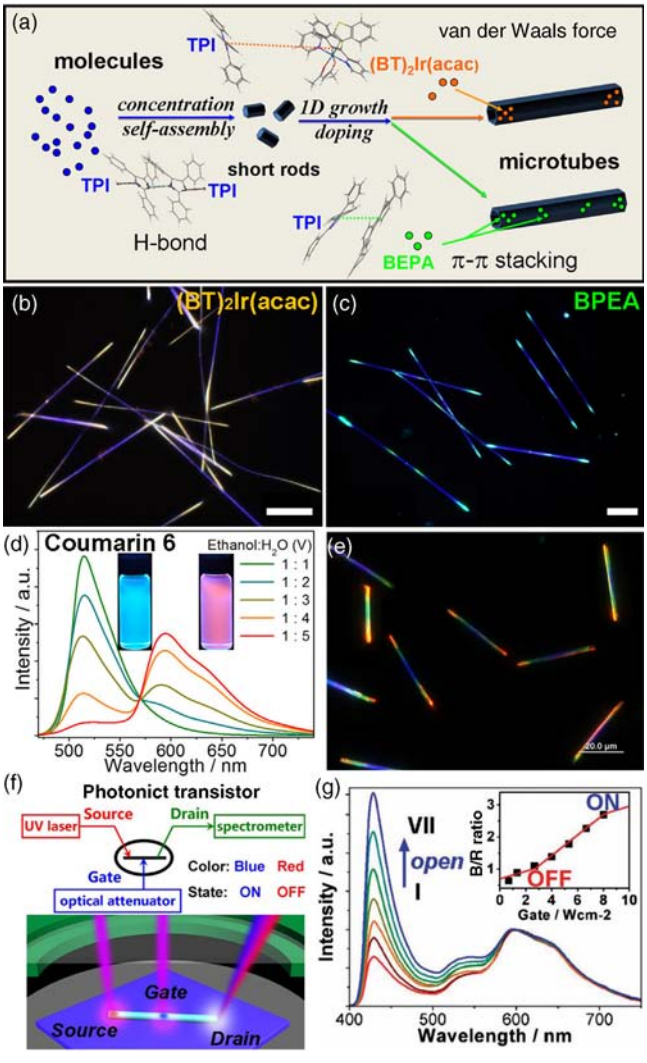

Figure 5.12 Formation and optical properties of the gradiently doped 1D nanostructures. (a) Schematic illustration for the formation of doped TPI tubes with different guest molecules. (b and c) PL microscopy images of the triblock and multiblock doped TPI microtubes. (d) Fluorescence spectra of coumarin 6 aggregates with different contents in the ethanol/water mixture. (e) PL microscopy image of coumarin 6-doped TPI microtubes. (f) Schematic illustrations of the design concept (top) and realization (down) of a photonic transistor in rainbow colored microtubes. (g) Outcoupled emission spectra from the drain port under various gate controls. Inset shows the relationship between outputted blue to red light ratio and the power of the gate laser. ((a–c) Copyright 2012, Wiley; (d–g) copyright 2013, Wiley.)

The formation mechanism of the TPI–coumarin 6 microstructures is similar to that of the TPI–$(BT)_2Ir(acac)$ pair. The doping gradient of coumarin 6 in the axial direction induced the full-colored photoluminescence along these microtubes (Figure 5.12e). Upon an unfocused UV light excitation, both TPI and coumarin 6 could be excited and emit fluorescence with different colors. A part of the emitted fluorescence is confined and self-guided in both directions. During the light propagation along the tubes, the irreversible energy transfer from the donor to the acceptor ensures a unidirectional light transfer in the optical materials. Such a characteristic is of great importance in the development of essential photonic devices, especially all-optical diodes and triodes.

The design concept and experimental verification of a photonic triode are illustrated in Figure 5.12f. The optical triode also constitutes source, drain, and gate components, which is similar to an electronic analogy. The incident laser excitation with a fixed intensity at the left end acts as the source, while the outcoupled light from the right tip is regarded as the drain. The gate beam with different attenuations is located at the middle part of the individual tube to control the conducting signal from the source to the drain. The outcouplings from the drain (Figure 5.12g) are gradually altered from red (blue/red < 1, OFF) to blue (blue/red > 1, ON) with increased gate intensity. The continuous blue/red ratio suggests a precise gate-modulated output of the transistor.

5.4.2.3 Core/Sheath Structures

Assembled organic crystalline nanomaterials are all excellent waveguides as the fluorescence can be well confined and propagated within the 1D structure due to the difference in refractive index between material and surrounding medium, which is mostly air. Ambient environmental changes could be recorded by the transmitted light in form of light parameters. Since light transmission in nanosized structures is very sensitive to the surrounding variance, such a mechanism could be applied to fabricate ingenious sensors. Figure 5.13 gives an example of photonic gas transducer with a single core/sheath nanowire, which was fabricated by decorating the single crystalline BPEA nanowire with chemoreactive bis(2,4,5-trichloro-6-carbopentoxyphenyl) oxalate (CPPO) [50]. A cooperative assembly method was put forward to get this core/sheath nanostructure (Figure 5.13a). The cable-like structures appeared with the proper ratio of BPEA to CPPO quantity so that the BPEA nanowires can be totally wrapped by the dye-doped CPPO shell, as testified by the TEM image in Figure 5.13b. The CPPO in the peripheral layer is highly sensitive and selective to the H_2O_2 gas as a typical chemiluminogenic compound. Such a core/sheath structure could not only keep the high chemical activity of CPPO, but also improve its mechanical and optical properties through the introduction of BPEA crystalline wire in the inner core.

A single nanowire heterostructure was employed as a gas sensor based on a gas concentration-dependent evanescent energy leakage (Figure 5.13c). The fluorescence under a laser excitation serves as the input signal while the outcoupled light is regarded as the output signal. Once the surrounding medium contains trace amounts (several ppm) of H_2O_2, the output coupling is drastically attenuated

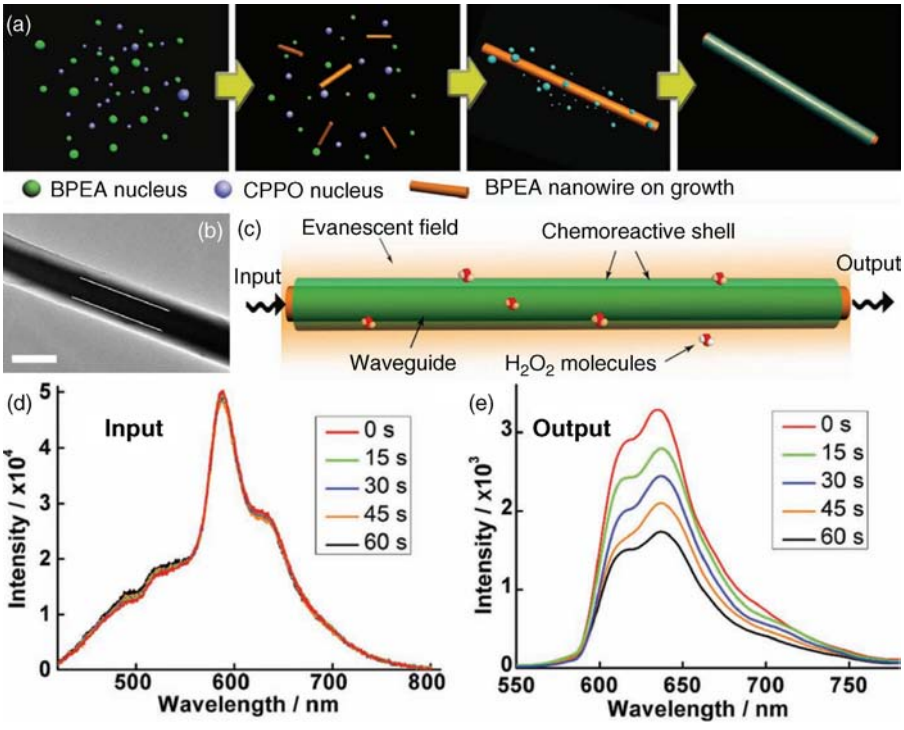

Figure 5.13 Formation and photonic sensing performance of the core/sheath nanostructure. (a) Scheme of the growth mechanism. (b) TEM image of a single core/sheath nanowire. Scale bar is 1 μm. (c) Schematic illustration for the evanescent field sensing of the core/sheath optical waveguide. Light is coupled into the cavity and travels through the sensing region coated with chemoreactive shell. (d and e) Time-dependent PL intensities of the input and output light on exposure to 6 ppm H_2O_2 vapor. (Copyright 2012, Wiley.)

(about 50%) while the input intensity remains unchanged (Figure 5.13d and e). The characteristic response of the nanowires exposed to the gas vapors is remarkably fast (tens of seconds). This cable-like optical waveguide sensing platform complements the present gas sensor with the ability of rapidly and specifically monitoring the amplified environmental variations, demonstrating the great potential of a single nanocable for on-chip optical probes. The use of a facile assembly method to obtain cable-like composites not only bestows the transducer with a defect-free structure and high sensitivity, but also enables the large-scale preparation, which is a key point to commercial products.

5.5 Conclusions

The ever-increasing demand of multifunctional photonic devices at micro-/nanoscale greatly promotes the development of chemistry and materials.

Organic materials are promising building blocks due to the huge advantages of flexible design, tailored properties, easy processability, and low cost. Small molecules tend to assemble into low-dimensional crystals impelled by the weak intermolecular interactions, resulting in unique photophysical and photochemical characteristics with large differences from their inorganic counterparts. Structure-dependent photonic properties have been demonstrated with these organic nanocrystals, suggesting a way to obtain desired functionalities. Till date, various improved construction strategies starting from organic molecules have been proposed continuously for the acquisition of functional materials.

However, systemic studies on the relationships among molecular design, assembly process control, morphological modulation, and optical performance manipulation of final products are rather scattered and suffer from an in-depth summarization. Considering these aspects, we began with a comprehensive introduction of the assembly process of several representative molecules, highlighting the influences of molecular interactions and environmental conditions on the molecular packing mode. Either aggregation in the liquid phase or epitaxial growth in the vapor phase has been proved to be a universal and facile preparation method to achieve diverse nanostructures.

Rational molecular design and targeted assembly method selection are higher demands of function-oriented material synthesis. On the basis of an in-depth understanding of basic assembly rules, we could tailor the intermolecular interactions by modifying the molecular structure or altering the environmental conditions, which may affect both the structures and properties of organic aggregations. A good way to obtain multifunctional materials is the construction of crystalline nanocomposites through cooperative assembly of several compounds, due to the ease of preparation and flexibility. Multicomponent materials, with the guest molecules uniformly or gradiently distributed in the nanostructures, have been demonstrated to be beneficial for high quality and performance in the application of the devices. Before that, it is imperative to precisely design and control the structures according to the desired properties. Besides photonic elements, the resulting composite nanomaterials could also be used in biomedicine, sensors, automation, optoelectronics, and so on.

So far, the development of organic nanomaterials is still far behind that of the inorganic counterparts, although considerable attention has been paid in the past few decades. The preparation of micro-/nanocrystals is still in its early stage, not to mention controllability. For this reason, a continuous investigation of molecular assembly would be necessary to develop improvements in reproducibility, uniformity, structural controllability, crystalline quality, and performances. In this sense, we hope to promote a comprehensive understanding of the relationships among molecules, assembly, structures, and properties to speed up the spiraling development of organic nanophotonic materials (Figure 5.14). Benefiting from the present developments, we know that optical performances of organic aggregates can be finely

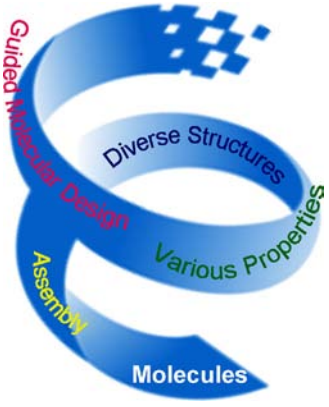

Figure 5.14 A spiraling cognition of the relationships among molecules, assembly, structures, and properties to power the following development of organic nanophotonic materials and devices.

tuned through rational molecular design and fabrication strategy selection. New efforts based on current cognitions would help us to achieve a better comprehension of the function-oriented assembly behavior as well as structure evolution, which would further stimulate progress in this area. A reasonable theoretical model, which is not limited to several molecules, will be beneficial for obtaining overall knowledge of the assembly process and structural confinement effect.

Present photonic devices primarily take advantage of the linear optical properties only, especially photoluminescence. It is not an easy thing to realize some sophisticated applications solely with the linear response, such as ultrafast switcher or signal amplifier. Thus, organic nanostructures consisting of large nonlinear optical molecules would be an appropriate alternative in such areas. The response time of nonlinear effect is usually on the order of femtoseconds to picoseconds. Such a rapid response pledges a good signal processing speed. Moreover, the nonlinear properties of organic materials might be magnified at micro-/nanoscale due to the size-dependent optical confine effect, facilitating the design and realization of nonlinear photonic devices.

Considering the vast number of organic species and great possibilities of their structure-related optical properties, it is reasonable to believe that there will be a brighter future for the organic assemblies as photonic materials. To achieve this goal, we need to devote ourselves to explore this promising field, especially the relationships among molecule, morphology, and performance. There are still many challenges, for example, synthesis of hierarchical structures, acquisition of complex functions, and synergistic effects among different compositions. We hope that the bottom-up assembly method will open up a new prospect for the creation of novel photonic materials.

Acknowledgments

This work was supported by the National Natural Science Foundation of China (Nos. 21125315 and 21373241), the Ministry of Science and Technology of China (2012YQ120060), and the Strategic Priority Research Program of the Chinese Academy of Sciences (Grant No. XDB12020300).

References

1 Kirchain, R. and Kimerling, L. (2007) A roadmap for nanophotonics. *Nat. Photon.*, **1** (6), 303–305.
2 Piccione, B., Cho, C.-H., van Vugt, L.K., and Agarwal, R. (2012) All-optical active switching in individual semiconductor nanowires. *Nat. Nanotechnol.*, **7** (10), 640–645.
3 Clark, J. and Lanzani, G. (2010) Organic photonics for communications. *Nat. Photon.*, **4** (7), 438–446.
4 Zhao, Y.S., Fu, H., Peng, A., Ma, Y., Liao, Q., and Yao, J. (2009) Construction and optoelectronic properties of organic one-dimensional nanostructures. *Acc. Chem. Res.*, **43** (3), 409–418.
5 Zhao, Y.S., Fu, H., Peng, A., Ma, Y., Xiao, D., and Yao, J. (2008) Low-dimensional nanomaterials based on small organic molecules: preparation and optoelectronic properties. *Adv. Mater.*, **20** (15), 2859–2876.
6 Avestro, A.-J., Belowich, M.E., and Stoddart, J.F. (2012) Cooperative self-assembly: producing synthetic polymers with precise and concise primary structures. *Chem. Soc. Rev.*, **41** (18), 5881–5895.
7 Lehn, J.-M. (2002) Self-organization and complex matter. *Supramol. Sci.*, **295** (5564), 2400–2403.
8 Cordovilla, C. and Swager, T.M. (2012) Strain release in organic photonic nanoparticles for protease sensing. *J. Am. Chem. Soc.*, **134** (16), 6932–6935.
9 Hong, Y., Lam, J.W.Y., and Tang, B.Z. (2011) Aggregation-induced emission. *Chem. Soc. Rev.*, **40** (11), 5361–5388.
10 Yan, Y. and Zhao, Y.S. (2012) Exciton polaritons in 1D organic nanocrystals. *Adv. Funct. Mater.*, **22** (7), 1330–1332.
11 Yan, Y., Zhang, C., Yao, J., and Zhao, Y.S. (2013) Recent advances in organic one-dimensional composite materials: design, construction, and photonic elements for information processing. *Adv. Mater.*, **25** (27), 3627–3638.
12 Zang, L., Che, Y., and Moore, J.S. (2008) One-dimensional self-assembly of planar π-conjugated molecules: adaptable building blocks for organic nanodevices. *Acc. Chem. Res.*, **41** (12), 1596–1608.
13 Zhang, C., Zou, C.-L., Yan, Y., Hao, R., Sun, F.-W., Han, Z.-F., Zhao, Y.S., and Yao, J. (2011) Two-photon pumped lasing in single-crystal organic nanowire exciton polariton resonators. *J. Am. Chem. Soc.*, **133** (19), 7276–7279.
14 Basak, S. and Chandrasekar, R. (2011) Multiluminescent hybrid organic/inorganic nanotubular structures: one-pot fabrication of tricolor (blue–red–purple) luminescent parallepipedic organic superstructure grafted with europium complexes. *Adv. Funct. Mater.*, **21** (4), 667–673.
15 Mizuno, H., Haku, U., Marutani, Y., Ishizumi, A., Yanagi, H., Sasaki, F., and Hotta, S. (2012) Single crystals of 5,5′-bis (4′-methoxybiphenyl-4-yl)-2,2′-bithiophene for organic laser media. *Adv. Mater.*, **24** (42), 5744–5749.
16 Bernstein, J., Sarma, J.A.R.P., and Gavezzotti, A. (1990) Generation of unknown crystal phases for aromatic hydrocarbons by packing energy calculations. *Chem. Phys. Lett.*, **174** (3–4), 361–368.
17 Zhang, C., Zou, C.-L., Yan, Y., Wei, C., Cui, J.-M., Sun, F.-W., Yao, J., and Zhao, Y. S. (2013) Self-assembled organic crystalline microrings as active

whispering-gallery-mode optical resonators. *Adv. Opt. Mater.*, **1** (5), 357–361.

18 Huang, L., Liao, Q., Shi, Q., Fu, H., Ma, J., and Yao, J. (2010) Rubrene micro-crystals from solution routes: their crystallography, morphology and optical properties. *J. Mater. Chem.*, **20** (1), 159–166.

19 Takazawa, K. (2007) Micrometer-sized rings self-assembled from thiacyanine dye molecules and their waveguiding properties. *Chem. Mater.*, **19** (22), 5293–5301.

20 Zhang, X., Zhang, X., Zou, K., Lee, C.-S., and Lee, S.-T. (2007) Single-crystal nanoribbons, nanotubes, and nanowires from intramolecular charge-transfer organic molecules. *J. Am. Chem. Soc.*, **129** (12), 3527–3532.

21 Zhao, Y.S., Xu, J., Peng, A., Fu, H., Ma, Y., Jiang, L., and Yao, J. (2008) Optical waveguide based on crystalline organic microtubes and microrods. *Angew. Chem., Int. Ed.*, **47** (38), 7301–7305.

22 Zhao, Y.S., Yang, W., and Yao, J. (2006) Organic nanocrystals with tunable morphologies and optical properties prepared through a sonication technique. *Phys. Chem. Chem. Phys.*, **8** (28), 3300–3303.

23 Zhang, X., Zhang, X., Shi, W., Meng, X., Lee, C., and Lee, S. (2007) Single-crystal organic microtubes with a rectangular cross section. *Angew. Chem., Int. Ed.*, **46** (9), 1525–1528.

24 Dai, Z.R., Pan, Z.W., and Wang, Z.L. (2003) Novel nanostructures of functional oxides synthesized by thermal evaporation. *Adv. Funct. Mater.*, **13** (1), 9–24.

25 Zhao, Y.S., Xiao, D., Yang, W., Peng, A., and Yao, J. (2006) 2,4,5-Triphenylimidazole nanowires with fluorescence narrowing spectra prepared through the adsorbent-assisted physical vapor deposition method. *Chem. Mater.*, **18** (9), 2302–2306.

26 Huang, M.H., Mao, S., Feick, H., Yan, H., Wu, Y., Kind, H., Weber, E., Russo, R., and Yang, P. (2001) Room-temperature ultraviolet nanowire nanolasers. *Supramol. Sci.*, **292** (5523), 1897–1899.

27 O'Carroll, D., Lieberwirth, I., and Redmond, G. (2007) Microcavity effects and optically pumped lasing in single conjugated polymer nanowires. *Nat. Nanotechnol.*, **2** (3), 180–184.

28 Briseno, A.L., Mannsfeld, S.C.B., Ling, M. M., Liu, S., Tseng, R.J., Reese, C., Roberts, M.E., Yang, Y., Wudl, F., and Bao, Z. (2006) Patterning organic single-crystal transistor arrays. *Nature*, **444** (7121), 913–917.

29 Zhao, Y.S., Zhan, P., Kim, J., Sun, C., and Huang, J. (2010) Patterned growth of vertically aligned organic nanowire waveguide arrays. *ACS Nano*, **4** (3), 1630–1636.

30 Yao, W., Yan, Y., Xue, L., Zhang, C., Li, G., Zheng, Q., Zhao, Y.S., Jiang, H., and Yao, J. (2013) Controlling the structures and photonic properties of organic nanomaterials by molecular design. *Angew. Chem., Int. Ed.*, **52** (33), 8713–8717.

31 Cantekin, S., Balkenende, D.W.R., Smulders, M.M.J., Palmans, A.R.A., and Meijer, E.W. (2011) The effect of isotopic substitution on the chirality of a self-assembled helix. *Nat. Chem.*, **3** (1), 42–46.

32 Wang, Y., Fu, H., Peng, A., Zhao, Y., Ma, J., Ma, Y., and Yao, J. (2007) Distinct nanostructures from isomeric molecules of bis(iminopyrrole) benzenes: effects of molecular structures on nanostructural morphologies. *Chem. Commun.*, **16**, 1623–1625.

33 Park, S.K., Varghese, S., Kim, J.H., Yoon, S.-J., Kwon, O.K., An, B.-K., Gierschner, J., and Park, S.Y. (2013) Tailor-made highly luminescent and ambipolar transporting organic mixed stacked charge-transfer crystals: an isometric donor–acceptor approach. *J. Am. Chem. Soc.*, **135** (12), 4757–4764.

34 Zhao, Y.S., Fu, H.B., Hu, F.Q., Peng, A.D., Yang, W.S., and Yao, J. (2008) Tunable emission from binary organic one-dimensional nanomaterials: an alternative approach to white-light emission. *Adv. Mater.*, **20** (1), 79–83.

35 Lei, Y., Liao, Q., Fu, H., and Yao, J. (2010) Orange–blue–orange triblock one-dimensional heterostructures of organic microrods for white-light emission. *J. Am. Chem. Soc.*, **132** (6), 1742–1743.

36 Wang, H., Liao, Q., Fu, H., Zeng, Y., Jiang, Z., Ma, J., and Yao, J. (2009) $Ir(ppy)_3$ phosphorescent microrods and nanowires: promising micro-phosphors. *J. Mater. Chem.*, **19** (1), 89–96.

37 Liu, T., Li, Y., Yan, Y., Li, Y., Yu, Y., Chen, N., Chen, S., Liu, C., Zhao, Y., and Liu, H. (2012) Tuning growth of low-dimensional organic nanostructures for efficient optical waveguide applications. *J. Phys. Chem. C*, **116** (26), 14134–14138.

38 Chandrasekhar, N. and Chandrasekar, R. (2012) Reversibly shape-shifting organic optical waveguides: formation of organic nanorings, nanotubes, and nanosheets. *Angew. Chem., Int. Ed.*, **51** (15), 3556–3561.

39 Yan, Y., Zhang, C., Zheng, J.Y., Yao, J., and Zhao, Y.S. (2012) Optical modulation based on direct photon–plasmon coupling in organic/metal nanowire hetero-junctions. *Adv. Mater.*, **24** (42), 5681–5686.

40 Palermo, V., Schwartz, E., Finlayson, C.E., Liscio, A., Otten, M.B.J., Trapani, S., Müllen, K., Beljonne, D., Friend, R.H., Nolte, R.J.M., Rowan, A.E., and Samorì, P. (2010) Macromolecular scaffolding: the relationship between nanoscale architecture and function in multichromophoric arrays for organic electronics. *Adv. Mater.*, **22** (8), E81–E88.

41 Cui, Q.H., Jiang, L., Zhang, C., Zhao, Y.S., Hu, W., and Yao, J. (2012) Coaxial organic p–n heterojunction nanowire arrays: one-step synthesis and photoelectric properties. *Adv. Mater.*, **24** (17), 2332–2336.

42 Bu, L., Pentzer, E., Bokel, F.A., Emrick, T., and Hayward, R.C. (2012) Growth of polythiophene/perylene tetracarboxydiimide donor/acceptor shish-kebab nanostructures by coupled crystal modification. *ACS Nano*, **6** (12), 10924–10929.

43 Zheng, J.Y., Yan, Y., Wang, X., Zhao, Y.S., Huang, J., and Yao, J. (2012) Wire-on-wire growth of fluorescent organic heterojunctions. *J. Am. Chem. Soc.*, **134** (6), 2880–2883.

44 Zhang, Y., Dong, H., Tang, Q., Ferdous, S., Liu, F., Mannsfeld, S.C.B., Hu, W., and Briseno, A.L. (2010) Organic single-crystalline p–n junction nanoribbons. *J. Am. Chem. Soc.*, **132** (33), 11580–11584.

45 Zhang, C., Zheng, J.Y., Zhao, Y.S., and Yao, J. (2011) Self-modulated white light outcoupling in doped organic nanowire waveguides via the fluctuations of singlet and triplet excitons during propagation. *Adv. Mater.*, **23** (11), 1380–1384.

46 Zhang, J., Zou, Q., and Tian, H. (2013) Photochromic materials: more than meets the eye. *Adv. Mater.*, **25** (3), 378–399.

47 Liao, Q., Fu, H., Wang, C., and Yao, J. (2011) Cooperative assembly of binary molecular components into tubular structures for multiple photonic applications. *Angew. Chem., Int. Ed.*, **50** (21), 4942–4946.

48 Zhang, C., Yan, Y., Jing, Y.-Y., Shi, Q., Zhao, Y.S., and Yao, J. (2012) One-dimensional organic photonic heterostructures: rational construction and spatial engineering of excitonic emission. *Adv. Mater.*, **24** (13), 1703–1708.

49 Zhang, C., Yan, Y., Yao, J., and Zhao, Y.S. (2013) Manipulation of light flows in organic color-graded microstructures towards integrated photonic heterojunction devices. *Adv. Mater.*, **25** (20), 2854–2859.

50 Zheng, J.Y., Yan, Y., Wang, X., Shi, W., Ma, H., Zhao, Y.S., and Yao, J. (2012) Hydrogen peroxide vapor sensing with organic core/sheath nanowire optical waveguides. *Adv. Mater.*, **24** (35), OP194–OP199.